Received: November 18, 2023. Revised: January 29, 2024.

International Journal of
Intelligent Engineering & Systems

http://www.inass.org/

Performance Evaluation of 5G New Radio Polar Code over Different Multipath Fading Channel Models

Mohammed Hussein Ali[1]* **Ghanim A. Al-Rubaye[1]**

[1]*Electrical Engineering Department, Mustansiriyah University, Baghdad, Iraq*
* Corresponding author's Email: eeph005@uomustansiriyah.edu.iq

Abstract: The coding of channels is a core part of any communication network. Future wireless systems will need high performance codes with low complexity encoding and decoding in order to meet a wide variety of requirements, from running in highly dependable situations with short information messages and low code rates to running in high throughput scenarios with lengthy messages and high code rates. The investigation of polar codes in fading channels has important implications in the context of implementing polar codes in wireless communications. A significant development in the fields of information and coding theory, polar code allows for the flexible adjustment of code rates and block lengths without compromising error correction efficiency. Recently, the Third Generation Partnership Project (3GPP) New Radio (NR) group has supported polar codes to provide channel coding in the physical control channels of the 5G, wireless standard. Channel coding, which exists inside the physical layer, is essential in determining the latency and dependability of a communication system. However, error correction performance diminishes with shorter message durations. The polar encoding scheme can achieve channel capacity because it is based on the practical use of channel polarization operation. In this research, a polar code is included in the proposed system for data transmission over various multipath fading channel models (Nakagami-m, Rayleigh, and Lognormal fading channels) in the presence of AWGN, and in this design, the Successive Cancellation List (SCL) decoding algorithms for polar code are used in order for the suggested NR-polar QAM-OFDM system to perform better than the uncoded QAM-OFDM system. According to Monte Carlo simulations, QAM constellation NR-Polar-COFDM using LLRs computed due to the normal distribution over different types of channel PDFs performs better than the uncoded QAM-OFDM system in terms of bit error rat BER. To further enhance the system performance, CRC bits are used to enhance the efficiency of SCL decoding by improving distance characteristics. The simulation results show that BER is approximately 10-6 at SNR of 1dB in the AWGN channel, and in the multipath fading channel BER approaches 10-6 at SNR of 22.5dB in the Rayleigh and Nakagami-m fading channels, while in the lognormal fading channel at SNR of 14dB for short information block lengths at code rates (1/3) in the uplink and downlink control channels. The findings additionally confirm the superiority of Polar coding in the situation of transmitting information with short block lengths in the AWGN compared to the NR-LDPC-OFDM.

Keywords: Polar code, OFDM, Nakagami-m fading, BER, Successive cancellation list (SCL), QAM, 5G NR, Physical uplink shared channel (PUSCH), Forward error correction (FEC), Physical downlink control channel (PDCCH), OFDM, SNR.

1. Introduction

Arikan initially created the category of error-correcting codes known as polar codes in 2008. These codes are capacity-achieving because they can reach the maximum possible channel capacity in theory. Polar codes may be used to repair transmissions that have been corrupted by the signal's fading as it traverses a multipath fading channel. Polar codes are based on the concept of creating "good" and "bad" channels, with the former having a low error probability and the latter having a high one, by taking use of the channel's inherent symmetry. Once encoded, the data is transferred across the good channels, while the poor channels are utilized for error correction. As a consequence, we have a coding scheme that is both economical and effective,

performing almost as well as capacity even across multipath fading channels [1]. To create a polar code, one must first determine the channel re- liability values that correspond to each bit to be encoded. Given a code length and a certain signal-to-noise ratio, this identification may be reliably carried out. However, the 5G architecture predicts a wide range of code lengths, speeds, and channel conditions, making it impractical to have a unique reliability vector for each possible combination of these characteristics. This is why a lot of work has gone into the formulation of polar codes that are simple to implement and require relatively little in the way of description complexity while yet providing reliable error correction over a wide range of code and channel settings [2]. In 5G New Radio (NR), control and user application data will be multiplexed and sent through the Physical Uplink Shared Channel (PUSCH). The 5G NR standard specifies a channel topology that differs somewhat from the PUSCH channel provided by the 4G LTE standard [3]. More flexible pilot arrangements and support for both CP-OFDM and DFTs-OFDM wave forms are only two examples of the ways in which the 5G NR improves upon its predecessor in terms of adaptability and dependability, and in addition to the trade-off between spectral and power efficiency for 5G NR design, the article ignores the effects of phase noise, frequency offset, and channel estimate errors on waveform performance [4]. The filtered Orthogonal Frequency-Division Multiplexing (f-OFDM) method was included as part of the standard to increase performance at higher modulation orders, but this approach utilizes f-OFDM will decrease out-of-band emissions, but requires supplementary filtering and complexity, and may not surpass CP-OFDM in terms of spectrum efficiency [5]. Furthermore, improvements in Forward Error Correction (FEC) were mandated to change the Turbo Codes used in 4G LTE with Quasi-Cyclic Low Density Parity Check (QC-LDPC) codes [6,7], which have been shown to create higher transmission rates and offer chances for even more effective system implementations. As well as the broadcast channel, it is used for downlink and uplink control information (DCI/UCI) in the enhanced mobile broadband (eM-BB) scenario. Channel coding schemes for data channels in eMBB are alternatively configured to use flexible LDPC for all block sizes. Evolution of basic constraints on the Bhattacharyya parameters of bit channels [8] is the foundation on which the first polar codes were built and the code building procedure for binary-input channels is too complex to provide a heuristic approach. Alternatively, a polar code tailored to the Binary Erasure Channel (BEC) may be used for any channel with a capacity of C bits. In [1] these constraints are only shown for BI-DMS channels, but they might be extended to Binary Input Discrete Memoryless Symmetric (BI-AWGN) channels, which use an unlimited alphabet. The codes developed using such constraints work well, despite the fact that they are loose for many bit-channels and that more specific approaches are subsequently developed. This architecture has the lowest O(N) complexity of any known one (excluding the selection of K best among N metrics obtained). There are 2N1-1 operations involved, which correspond to the polarizing kernel transformation of upper bounds. Recent research [9], proposed construction method is based on the concept of recursive convolutional codes which is involve the encoding the information bits using a series of recursive convolutional codes, this widely used technique as well and this method attains a rate close to the theoretical maximum, surpasses current approaches, and has a complexity of O (N log N), demonstrating its efficacy.

In [1], a similar but older architecture is presented using Monte-Carlo simulation of the bit-channels. Channels with finite and infinite alphabets, such as AWGN, may benefit from this method. Tal and Vardy [10] suggested an updated building method, and provide analysis of building methods theoretically proves that linear polar codes may be produced within a reasonable amount of time and space, given set big code lengths, which built on the work of Mori and Tanaka [11,12], Bit channels were originally intended to be located using an analysis of their whole finite alphabet distributions, and the authors performed a comparison between the performance of polar codes using a novel building approach for arbitrary symmetric binary memoryless channels (B-MC) with linear complexity in the block length, and the heuristic method. The findings showed that the polar codes utilizing the new construction method outperformed the heuristic method. Once n channel modifications have been performed, the method becomes unsolvable since the alphabet size has grown to an N^{th} power (exponentially). Depending on a successive cancellation decoder (SCD) over a binary erasure channel (BEC), a systematic polar encoder (SPE) was proposed in [13] and demonstrated that BP decoding exhibited worse performance in comparison to SC decoding, especially at high signal-to- noise ratios. SC decoding is a distinct variant of BP decoding that follows a certain update schedule, indicating that other schedules may enhance the performance of BP decoding. In [14], a different encoder was suggested that used a two non-systematic polar encoder circuits are connected in a chain, it was shown recently that

this kind of encoder only performs in certain situations. They also indicate that in low error-rate zones, a polar code with a higher Eb/N0 of 4.5 dB is required to surpass the performance of the LDPC code. Furthermore, a combination of several polar codes may might surpass the LDPC code even in high error-rate regions. Although the polar code's decoder is lengthier, it has a lower level of implementation complexity. LDPC code even in high error-rate regions. Although the polar code's decoder is lengthier, it has a lower level of implementation complexity.

Using Arakan's algorithm, researchers propose a systematic encoder for general (l*l) triangular kernels with a memory of O(N), where N denotes the size of a block bits, and a sophistication of O (N log N). We notice that all of the above SPEs are more complicated, take up more memory, and have longer wait times than NSPEs. The OFDM communication system is an effective method of optimizing the utilization of the available spectrum. In this configuration, M-Q AM might significantly improve spectrum use. High-order modulation has the potential to increase the error rate of low-power transmission systems significantly. For this reason, OFDM systems commonly use FEC to lower the error rate, and the proposed method in [15] presents various drawbacks, such as heightened complexity and computational cost in MIMO-OFDM systems as a result of hybrid coding and decoding procedures, compatibility concerns with established standards and protocols, and potential inefficiency for higher-order MIMO-OFDM systems due to amplified interference and channel estimation errors. In order to convert the frequency-selective multipath into narrow band frequency-flat channels, OFDM is often employed in conjunction with a cyclic prefix (CP) to eliminate ISI [16]. An NR-Polar-QAM-OFDM system is develop- ped here, and its BER performance is evaluated and compared to that of uncoded QAM-OFDM systems over a multipath Rayleigh environment, Nakagami-m environment and Lognormal environment under the AWGN scenario. In a multipath channel scenario where the channels deteriorate progressively, our findings show that the Polar-COFDM system per- forms better than the uncoded OFDM system. The remaining parts of the article are structured in the following manner: The techniques used in the Polar Code are clarified in Section 2, providing a comprehensive background. Section 3 of the article provides an explanation of the 5G NR Polar Code system. We present our concept of the NR-Polar- OFDM system using the 3GPP 5G NR physical layer standard, and used the full PUSCH channel structure and full PDSCH channel structure. Synchronization, different channels, and symbol identification are only some of the receiver algorithms taken into account by the model in the section 4. Information on the computation of BER over Lognormal fading channel in the fifth section. The numerical evaluation of Polar-COFDM systems is presented in sixth section, where the simulation results are shown, we have also carried out a comparison of the coding gain with the LDPC OFDM system. The last portion presents the conclusions.

2. Background of polar code techniques

Channel polarization, a relatively new phenomena, provides the primary creative inspiration for the PC design. To implement channel polarization, N channels will be combined recursively, and then the resulting channel will be separated into N artificial sub-channels. In the best-case scenario, the iterative constructing procedure will provide sub-channels with a transmission capacity of 1, but in the worst-case scenario, the capacity will be close to 0. These excellent sub-channels will then be used to transmit significant data as part of the coding method, while the remaining unreliable sub-channels will be ignored.

2.1 Polar encoding process

Let's indicate the N-bit vector of information with the symbol, $s_1^N = (s_1, s_2, s_3, \dots\dots, s_N,)$. It is possible to get the polar codeword for the data vector s_1^N by using,

$$x_1^N = s_1^N F_N \tag{1}$$

Where F_N is generator matrix is determined by using [1,9]

$$F_N = A_N G^{\otimes n} \tag{2}$$

$G^{\otimes n}$ represents the Kronecker product of matrix G with itself n, in which case $N = 2^n$, G=$\begin{bmatrix}1 & 0\\ 1 & 1\end{bmatrix}$ and A_N is determined by using

$$A_N = H_N\left(I_2 \otimes A_{\frac{N}{2}}\right) \tag{3}$$

Where the H_N represent the $(N \times N)$ matrix of bit reversal and permutation, can be defined as

$$(s_1, s_2, s_3, \dots, s_N)H_N = (s_1, s_3, \dots, s_{N-1}, s_2, s_4, \dots, s_N) \tag{4}$$

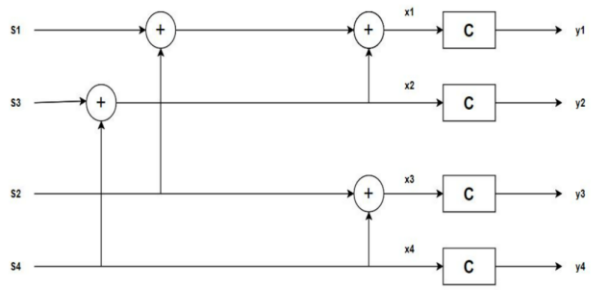

Figure. 1 Polar encoder for codeword length 4

Consider, as an instance: for (s_1,s_2,s_3,s_4), the H_4 matrix may be found by using

$$H_4 = \begin{bmatrix} 1 & 0 & 0 & 0 \\ 0 & 0 & 1 & 0 \\ 0 & 1 & 0 & 0 \\ 0 & 0 & 0 & 1 \end{bmatrix}$$

So, $(s_1, s_2, s_3, s_4,)H_4 = (s_1, s_3, s_2, s_4,)$

Using Eq. (2), the generator matrix of the polar code for N=4 can be computed as

$$F_4 = \begin{bmatrix} 1 & 0 & 0 & 0 \\ 1 & 0 & 1 & 0 \\ 1 & 1 & 0 & 0 \\ 1 & 1 & 1 & 1 \end{bmatrix}$$

Encoder hardware architecture is shown in Fig. 1, where C represents a channel for data transmission.

2.2 Polar decoding process

In order to decode a Polar code, the SC decoder uses a "successive cancellation" procedure to iteratively estimate the values of the bits. Based on the incoming signal and the decoder's prior estimations of the other bits, it determines the probability that each bit is either a 1 or a 0. The decoder utilizes that information to eliminate the impact of the unreliable information bits and boost the accuracy of the remaining bit estimations [1]. Soft information is initially sent to the decoder by the demodulator in the form of a log-likelihood ratio (LLR). Using the previously chosen bits $\hat{s}^{i-1}$, this algorithm calculates the likelihood ratio for the i[th] bit as

$$L_N^{(i)}\left(y_1^N, \hat{s}_1^{i-1}\right) = \frac{C_N^{(i)}(y_1^N, \hat{s}_1^{i-1} \rfloor s_i=0)}{C_N^{(i)}(y_1^N, \hat{s}_1^{i-1} \rfloor s_i=1)} \tag{5}$$

$$L_N^{(2i-1)}\left(y_1^N, \hat{s}_1^{2i-2}\right) = \frac{L_{\frac{N}{2}}^{(i)}\left(y_1^{\frac{N}{2}}, \hat{s}_{1,o}^{2i-2} \oplus \hat{u}_{1,e}^{2i-2}\right) L_{\frac{N}{2}}^{(i)}\left(y_{N/2+1}^N, \hat{s}_{1,e}^{2i-2}\right)+1}{L_{\frac{N}{2}}^{(i)}\left(y_1^{\frac{N}{2}}, \hat{s}_{1,o}^{2i-2} \oplus \hat{s}_{1,e}^{2i-2}\right)+L_{\frac{N}{2}}^{(i)}\left(y_{N/2+1}^N, \hat{s}_{1,e}^{2i-2}\right)} \tag{6}$$

and

$$L_N^{(2i)}\left(y_1^N, \hat{s}_1^{2i-1}\right) = \left[L_{\frac{N}{2}}^{(i)}\left(y_1^{\frac{N}{2}}, \hat{s}_{1,o}^{2i-2} \oplus \hat{s}_{1,e}^{2i-2}\right)\right]^{1-2\hat{s}_{2i-1}} L_{\frac{N}{2}}^{(i)}\left(y_{N/2+1}^N, \hat{s}_{1,e}^{2i-2}\right) \tag{7}$$

The expression $\hat{s}_{1,e}^{2i-2}$ (or $\hat{s}_{1,o}^{2i-2}$) represents a subset of $\hat{s}_1^{2i-2}$, consisting of elements with even (or odd) number of indexes.

When N is 1, the primary LLR is calculated using a formula.

$$L_1^1(y) = \frac{C(y_i|0)}{C(y_i|1)} \tag{8}$$

$$\hat{s}_i = \begin{cases} 0 & if \quad L_N^{(i)}\left(y_1^N, \hat{s}_1^{i-1}\right) \geq 1 \\ 1 & o.w. \end{cases} \tag{9}$$

where $L_N^{(i)}\left(y_1^N, \hat{s}_1^{i-1}\right)$ may be computed iteratively, as shown in (6) and (7).

For calculating the likelihood ratios in (6) and (7), a graphical butterfly structure is provided in [1]. The structure is too complicated to be suitable for processing in parallel. Therefore, suggested the use of a tree structure for the SC decoding process of polar codes [17]. The introduction of a list-based decoding strategy for polar codes, known as Successive Cancellation List (SCL), has been described in reference [18]. Multiple SC decoders keep many codeword possibilities simultaneously while they operate in parallel. Each time a leaf node has been reached, the bit is predicted to have both a value of 1 and a value of 0, resulting in a doubling of the number of feasible codewords. The path metric for every potential candidate is modified, taking into account the LLR value related with the node. The less probable alternatives are then eliminated in order to prevent the algorithm from becoming too complicated. The use of SCL significantly enhances the error-correction capabilities of SC for intermediate code lengths, particularly when the code is concatenated with a Cyclic Redundancy Check (CRC). The above technique has been used as a fundamental reference point in the assessment of error-correction performance in the context of 5G technology.

3. 5G NR polar code scheme

Every possible channel in the physical world introduces unwanted noise, which in turn causes errors and lowers the system's dependability. Channel coding, which enhances the robustness of digital communication systems by including redundancies in the transmitted data in a managed

fashion, [19]. Here, we provide a detailed description of the 5G standard's accepted structure for the encoding of polar codes. The format specified by the 3GPP technical standard will be used in the following [20]. Where Uplink Control Information (UCI) is encoded using polar codes for transmitting on the PUCCH and the PUSCH. Payloads in the physical broadcast channel and the downlink control information (DCI) via the physical downlink control channel (PDCCH) are encoded using polar codes (PBCH).

In 5G scenarios, the number of bits in the information is fixed at A, and a codeword of length E code bits is transmitted to reach the needed rate R = A/E, for the higher-level communication layers. When combined with the information bits, the L CRC bits provide a total of K bits, which are then encoded using a (N, K) mother polar code. In order for polar codes to conform to this criterion, a mother polar code of length $N = 2^n$ is first generated, and then the code length E is matched by puncturing, shortening, or repeating and to reach the rate R. Mother code length N has a minimum of 32 bits (N_{min}) and a maximum of 512 bits (N_{max}) for downlink and 1024 bits (N_{max}) for uplink, respectively. The lowest acceptable coding rate of (1/8) require an additional upper restriction. The A data bits that will be conveyed through the code of length E are stored in vector a. Messages may be segmented and divided into two group, each of which can be encoded independently yet sent concurrently, depending on the coding specifications. The resultant vector C, which is made up of CRC bits which are added at the end of the data bits which is consisting of K = A + L bits, is routed via an interleaver.

A mother polar code of length N is created, together with the relative bit channel reliability pattern and frozen group, based on the required code rate R and codeword length E. The N-bit s vector's remaining bits are frozen, and the interleaved vector c, which may also include parity-check bits, is given to the information set. After deciding on a mother code, the vector s is encoded as (1). After encoding, x is split into 32 blocks of equal length by a subblock interleaver, and the resulting scrambled output, producing y, which is then inserted into the circular buffer. Using puncturing, shortening, or repeating, we can transform the N-bit vector y into an E-bit vector e, and then can use a channel interleaver to calculate the vector c, which can be modulated and then trans- mitted as the c. after concatenation, if required. The 5G encoding procedures are shown in Fig. 2, for the downlink. While the Fig. 3 shows diagram of the uplink transmit end processing, with essential components and their parameters indicated,

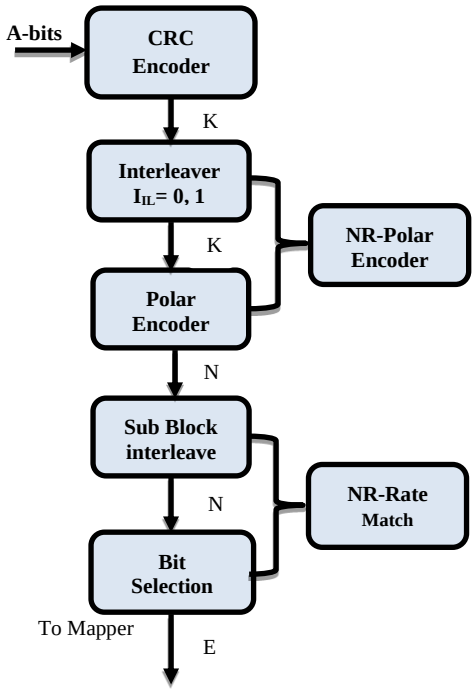

Figure. 2 The 5G NR- DCI encoding scheme

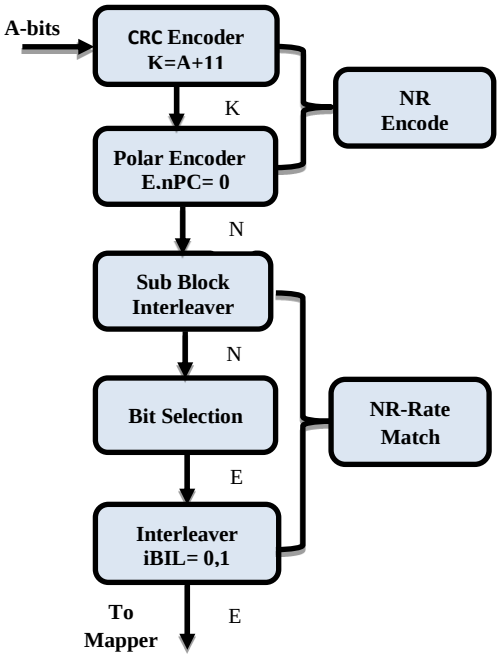

Figure. 3 The 5G NR- UCI decoding scheme

with a payload size higher than 19 bits and no code-block segmentation.

A vector c of A + L bits is created by adding an L-bit CRC to the A message bits that were previously stored in a. The potential generator polynomials for CRC are as follows:

$$f_6(D) = D^6 + D^4 + 1$$
$$f_{11}(D) = D^{11} + D^{10} + D^9 + D^1 + 1$$

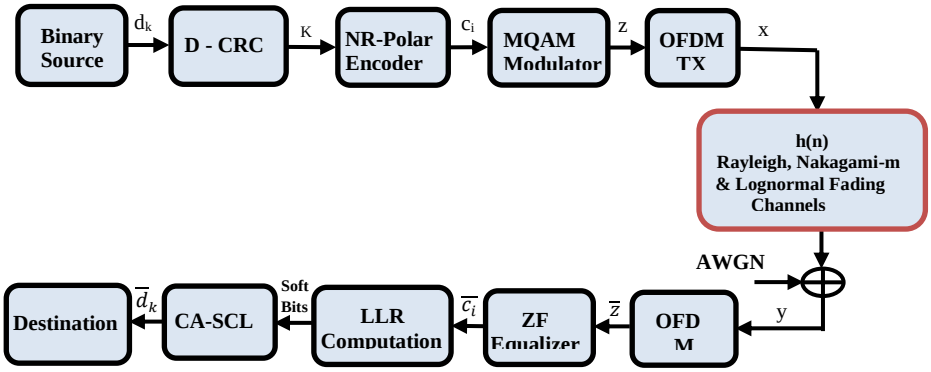

Figure. 4 Schematic structure NR-Polar Code QAM-OFDM

$$f_{24}(D) = D^{24} + D^{23} + D^{21} + D^{20} + D^{17} + D^{15} + D^{13} + D^{12} + D^{8} + D^{4} + D^{2} + D + 1$$

In the PBCH and PDCCH, the polynomial $f_{24}(D)$ is employed for the payload and DCIs, respectively. On the other hand, polynomials $f_6(D)$ and $f_{11}(D)$ are utilized for UCIs when the value of A falls within the range of 12 to 19, and when A is greater than or equal to 20, respectively.

4. 5G NR Polar-COFDM system model

The architecture of our 5G New Radio (NR) Polar-COFDM system is shown in Fig. 4. In the subsections that follow, we'll break down main parts of the system's block diagram and explain what it does.

4.1 Transmitter

The system's transmitter consists of an inverse fast Fourier transform (IFFT) component, an M-QAM digital modulator, a cyclic prefix block, and a polar encoder. The order of bits in the input is assumed to be completely random and statistically independent. A polar code is used to encode the input sequence of bits ($d = d_0, d_1, \ldots, d_{k-1}$). Both capacity-approaching codes have the same encoding rate of 0.5, and 0.333.

The output of the NR-Polar encoder ($c_i = c_o, c_1, \ldots, c_{n-1}$), is sent into a digital modulator, where it is rearranged into various patterns, such as the 4-QAM format, where two coded bits are merged to make a single symbol. Just as how one 16-QAM symbol is generated by combining four groups of coded bits. Under the grey mapping constellation, the coded bits are joined to generate the matching symbol, Therefore, the appropriate QAM symbol for a k-tuple $\{ c_m, c_{m+1}, \ldots c_{m+k+1} \}$ of bits, is,

$$X_k = \boldsymbol{C}\left[\sum_{m=0}^{k-1} 2^{k-1-m}\, c_m\right] \qquad (10)$$

The symbol $\boldsymbol{C} \in \mathbb{C}^{1X2^k}$ represents the vector of Gray-encoded in the time domain.

A serial-to-parallel converter receives the digitally modulated symbol of code bits c_i and makes it possible to process the symbols c_i in parallel that is in a serial fashion. The frequency domain is therefore represented by the symbols c^f[i] where i = 1, 2,.... When an IFFT is applied, the signal that comes out is the time domain signal that corresponds to $, c^t$ [i] to facilitate transmission, the parallel signal is c^t [i] converted back to its serial form. An N-points IFFT may be used to create a complex OFDM signal in the baseband, as shown in Eq. (11).

$$x_n = \frac{1}{\sqrt{N}} \sum_{k=0}^{N-1} X_k \exp\left(\frac{2j\pi kn}{N}\right), \quad n = 0,1,\ldots,N-1 \qquad (11)$$

The phenomenon of ISI caused by multipath propagation has affected the entire conventional wireless communication systems.

In order to exceed the maximum delay spreading of channel (L_d), a time-domain cyclic prefix (CP) with a duration of N_{CP} samples is employed. This CP is introduced at the beginning of each OFDM symbol by duplicating the final N_{CP} samples of the IFFT output x_n and appending them to the start of x_n. As a result, the transmitted symbols $\tilde{x} = [x_{N-N_{CP}}, x_{N-N_{CP}+1}, \ldots, x_{N,}\ x_o, x_1, \ldots, x_{N-1}]$, have a total length of $N_l = N + N_{CP}$ samples . This technique effectively reduces the influence of ISI that occurs between consecutive OFDM signals within channels. The aforementioned carriers traverse a diverse range of fading channels, whereby each channel introduces its own distinct noise at the point of reception. This noise contributes to the signal as shown in Eq. (12).

4.2 Multipath channel model

Fundamental to the study of communication theory is the assumption of some degree of noise distortion in transmitted signals. In most cases, it is

supposed that the noise AWGN. A more realistic scenario for wireless communications is the possibility of several paths connecting transmitters and receivers. These routes may be direct or generated by processes including reflection, diffraction, and scattering. The gathered signal is a vector of individual delayed signals, each of which has its own frequency, amplitude, and delay [21, 22].

For short-term or localized fades, the Rayleigh and Rician distributions are useful, but the lognormal distribution is better suited to explain longer-term or global phenomena. On the other hand, Nakagami's m-distribution [23] is a more adaptable statistical model that can replicate both the Rayleigh and the one-sided Gaussian fading scenarios. Furthermore, at certain intervals on the mean rating scale, the Nakagami distribution may serve as a suitable approximation to the log-normal and Rician distributions [16, 24, 25]. The Nakagami and Rician distributions are a better fit for low signal-to-noise levels (SNRs) than they are for high SNRs. The Nakagami distribution also gives a better fit to experimental data over a broad range of physical propagation of the channels, and it is more flexible than the log-normal and Rician distributions [16, 25, 26]. The performance of a system will suffer greatly if fading occurs.

4.2.1 Rayleigh fading channel

The flat fading channel model is the one that is used the most often for limited bandwidth transmission via mobile and wireless channels. The flat fading channel reduces the strength of all of the individual frequency components of the signal by the same degree. Because of this, the received signal, which was in its complex baseband form, may be expressed as [16, 24, 27]

$$y = \alpha x + u \tag{12}$$

y represents the signal that was received and x represents the symbol that was sent, u , is AWGN amplitude, and α the fading channel coefficients. A stochastic function is the amplitude of the fade, which is represented by the symbol "α" The channel exhibits nothing but AWGN when there is no fading at all (α = 1). If the amplitude of the fading channel adheres to the Rayleigh distribution, then the probability distribution $P(|\alpha|)$ may be written as the following [27-28]:

$$f_\alpha(\alpha) = \frac{\alpha}{\sigma_h^2} \exp\left(-\frac{\alpha^2}{2\sigma_h^2}\right) \tag{13}$$

In this situation, the inphase and quadrature phase components will both have distributions that are Gaussian with $N(0, 1/2)$ as[27]:

$$f_\alpha(\alpha^I) = \frac{1}{\sqrt{2\pi\sigma_h^2}} \exp\left(-\frac{(\alpha^I)^2}{2\sigma_h^2}\right), -\infty \le \alpha^I < \infty \tag{14}$$

$$f_\alpha(\alpha^Q) = \frac{1}{\sqrt{2\pi\sigma_h^2}} \exp\left(-\frac{(\alpha^Q)^2}{2\sigma_h^2}\right), -\infty \le \alpha^Q < \infty \tag{15}$$

Where σ_h^2 indicate to the typical strength of the received signal, which depends on the path of loss and the shadowing alone.

4.2.2 Nakagami-m fading channel

The Nakagami-m distribution combines the most advantageous aspects of the Rayleigh and Rician distributions. Nakagami provides a better match to the data from a mobile communication channel than the Rayleigh and Rician models by providing a fuller explanation to both less severe and more extreme scenarios. Nakagami-m is often seen as a generalization of the Chi-distribution. In mathematics, it is similar to the chi squared having 2m degrees of freedom [29].

Nakagami-m also offers the best possible fit for the transmission of radio waves from spacecraft to terrestrial structures. To characterize the rate of fading in this case, we make use of a parameter designated as the m parameter or parameter shape. The amount of fading attributable to scattering and multipath interference may be estimated using this parameter. Because of this, we may define the fading channel's amplitude in the time domain according to the Nakagami-m distribution as [16, 24,27]:

$$f_\alpha(\alpha) = \frac{2m^m}{\Gamma(m)\Omega^m}\alpha^{2m-1}\exp\left(-\frac{m\alpha^2}{\Omega}\right), \quad 0 \le \alpha < \infty, \quad m \ge 0.5 \tag{16}$$

Where, $\Omega = 2\sigma^2$ is the mean power of the multipath scatter zone. The symbol " α " denotes the strength of the signal that was received, and shape parameter is denoted by m. When m equals one, the distribution becomes identical to the Rayleigh distribution, where represents the inverse of the normalized variance of α^2. This distribution is typically the best fit for simulating land-mobile and indoor multipath propagation.

Given this scenario, $\alpha = \alpha^I + j\alpha^Q$, where $\alpha^I = |\alpha|\cos(\theta)$ and $\alpha^Q = |\alpha|\sin(\theta)$. The distribution of the inphase component and the quadrature phase component can be expressed as [27],

$$f_\alpha(\alpha^I) = \frac{2m^m}{\Gamma(m)|\cos(\theta)|\Omega^m}\left(\frac{\alpha^I}{\cos(\theta)}\right)^{2m-1}\exp\left(-\frac{m(\alpha^I)^2}{\Omega\cos(\theta)^2}\right), \quad (17)$$
$$-\infty \le \alpha^I < \infty$$

$$f_\alpha(\alpha^Q) = \frac{2m^m}{\Gamma(m)|\sin(\theta)|\Omega^m}\left(\frac{\alpha^Q}{\sin(\theta)}\right)^{2m-1}\exp\left(-\frac{m(\alpha^Q)^2}{\Omega\sin(\theta)^2}\right), \quad (18)$$
$$-\infty \le \alpha^Q < \infty$$

4.2.3 Log-normal fading channel

The quality of the connection may be negatively impacted in terrestrial and satellite land-mobile systems by gradual variations in the mean signal strength that are brought on by the shadowing that is caused by topography, buildings, and trees. The performance of the communication system will only be dependent on shadowing if the radio receiver has the ability to average out the rapid multipath fading or if a reliable "micro" diversity network is employed to reduce the impact of multipath. On the basis of actual observations, there is widespread agreement that shadowing can be represented by a log-normal distribution for a variety of situations, both indoors and outdoors [30-32]. In this scenario, the route SNR per symbol α will have a PDF that is provided by the conventional log-normal equation. As a result, the amplitude of the fading channel in the time domain follows the log-normal distribution and is described as:

$$f_\alpha(\alpha^r) = \frac{A_o}{\alpha^r\sqrt{2\pi}\sigma}\exp\left(-\frac{(10\log_{10}\alpha^r-\mu)^2}{2\sigma^2})\right), \quad (19)$$

Where $0 \le \alpha^r < \infty$, $A_o = 10/log_e 10$,
The equation (17), which can alternatively be represented as:

$$f_\alpha(\alpha^r) = \frac{1}{\alpha^r\sqrt{2\pi\sigma^2}}\exp\left(-\frac{(\ln(\alpha^r-\mu))^2}{2\sigma^2})\right), \quad (20)$$

Where $0 \le \alpha^r < \infty$, and r = {I, Q} indicate to the real component and imaginary component, respectively. μ and σ^2 are the mean and variance of the Gaussian R.V, in decibel units respectively, i.e. in α^r. The probability density function (pdf) of the variable in decibels will be Gaussian if the lognormal variable is changed to decibel units.
After performing an FFT operation in the frequency domain, the distribution of the real and imaginary components of the channel distribution in Eq. (20) will become closer and closer to a normal distribution, as stated by the central limit theorem (CLT), i.e. $f_\alpha(\alpha^r) = N(\alpha^I, 0, {\sigma_{LN}}^2)$ and $f_\alpha(\alpha^r) = N(\alpha^Q, 0, {\sigma_{LN}}^2)$ where $\boldsymbol{\alpha}^I$ and $\boldsymbol{\alpha}^Q$ are zero-mean statistically independent orthogonal Gaussian R.V. utilizing the value of Eq. (20) to determine the variance.

$$P_{DGmin} \le P_{DG} \le P_{DGmax} \quad (21)$$

$${\sigma_{LN}}^2 = E\{|\alpha^r|^2\} - (E\{|\alpha^r|\})^2 \quad (22)$$

$${\sigma_{LN}}^2 = \int_0^\infty (\alpha^r)^2 f_\alpha(\alpha^r)d\alpha^r - \int_0^\infty \alpha^r f_\alpha(\alpha^r)d\alpha^r)^2 \quad (23)$$

$${\sigma_{LN}}^2 = \int_0^\infty \frac{\alpha^r}{\sqrt{2\pi\sigma^2}}\exp\left(-\frac{(\ln(\alpha^r-\mu))^2}{2\sigma^2})\right)d\alpha^r - (\int_0^\infty \frac{1}{\sqrt{2\pi\sigma^2}}\exp\left(-\frac{(\ln(\alpha^r-\mu))^2}{2\sigma^2})\right)d\alpha^r)^2 \quad (24)$$

Let $a = \frac{1}{\sqrt{2\pi\sigma^2}}, b = \frac{1}{2\sigma^2}$ and $\text{erf}(\alpha^r) = \frac{2}{\sqrt{\pi}}\int_0^\infty e^{-z^2}dz$

$${\sigma_{LN}}^2 = \frac{\sqrt{\pi}a\, e^{\frac{1}{b}+2\mu}}{2\sqrt{b}}\text{erf}\left(\frac{-b\mu + blog(\alpha) - 1}{\sqrt{b}}\right)|_0^\infty - (\frac{\sqrt{\pi}a\, e^{\frac{1}{4b}+\mu}}{2\sqrt{b}}\text{erf}\left(\frac{-2b\mu+blog(\alpha)-1}{2\sqrt{b}}\right)|_0^\infty)^2 \quad (25)$$

$${\sigma_{LN}}^2 = \frac{\sqrt{\pi}a\, e^{\frac{1}{b}+2\mu}}{2\sqrt{b}} - \left(-\frac{\sqrt{\pi}a\, e^{\frac{1}{b}+2\mu}}{2\sqrt{b}}\right) - (\frac{\sqrt{\pi}a\, e^{\frac{1}{4b}+\mu}}{2\sqrt{b}} - \left(-\frac{\sqrt{\pi}a\, e^{\frac{1}{4b}+\mu}}{2\sqrt{b}}\right))^2 \quad (26)$$

$${\sigma_{LN}}^2 = \frac{\sqrt{\pi}\sqrt{2\sigma^2}}{\sqrt{2\pi\sigma^2}}e^{2\sigma^2+2\mu} - (\frac{\sqrt{\pi}\sqrt{2\sigma^2}}{\sqrt{2\pi\sigma^2}}\, e^{\frac{2\sigma^2}{4}+\mu})^2 \quad (27)$$

$${\sigma_{LN}}^2 = e^{2\sigma^2+2\mu} - (e^{\left(\frac{\sigma^2}{2}\right)+\mu})^2 \quad (28)$$

$${\sigma_{LN}}^2 = e^{2\mu}\left(e^{2\sigma^2} - e^{\sigma^2}\right) \quad (29)$$

4.3 Receiver

After the removal of the guard interval, the demodulation of the OFDM carrier is carried out by the implementation of a FFT [33]. This mathematical operation facilitates the conversion of the signal from the time domain to the frequency domain. The Eq. (12) represents the complex signal at the receiver, which may be represented in the frequency domain as follows [27, 34-35]:

$$Y^I + jY^Q = (Z^I + jZ^Q).(X^I + jX^Q) + U^I + \text{j}U^Q \quad (30)$$

In the frequency domain, the symbols Y, Z, X, and U represent the following entities: Y denotes the complex received signal, Z represents the transfer function of the complex fading channel, X stands for the complex modulated signals, and U signifies the AWGN. As per the CLT, the real component and the imaginary part's distributions tend to approximate a Gaussian distribution subsequent to the FFT operation. The mean of these distributions is zero, but the variance is based on the specific channel used. For the Rayleigh fading channel, the PDF (Z^I) and the PDF (Z^Q) may be represented as (14) and (15). In the context of the Nakagami-m fading channel, the probabilities $P(Z^I)$ and $P(Z^Q)$ may be mathematically represented as [27]

$$f_Z(Z^I) = \frac{1}{\sqrt{2\pi\sigma_N^2}} \exp\left(-\frac{(Z^I)^2}{2\sigma_N^2}\right), -\infty \le A^I < \infty \quad (31)$$

$$f_Z(Z^Q) = \frac{1}{\sqrt{2\pi\sigma_N^2}} \exp\left(-\frac{(Z^Q)^2}{2\sigma_N^2}\right), -\infty \le A^Q < \infty \quad (32)$$

Where σ_N^2 is the variance of the Nakagami-m fading channel, $\sigma_N^2 = \Omega\left(1 - \frac{1}{m}\left(\frac{\Gamma(m+\frac{1}{2})}{\Gamma(m)}\right)^2\right)$.

The $P(Z^I)$ and $P(Z^Q)$ for the Lognormal Fading Channel may be expressed mathematically as

$$f_Z(Z^I) = \frac{1}{\sqrt{2\pi\sigma_{LN}^2}} \exp\left(-\frac{(Z^I)^2}{2\sigma_{LN}^2}\right), -\infty \le A^I < \infty \quad (33)$$

$$f_Z(Z^Q) = \frac{1}{\sqrt{2\pi\sigma_{LN}^2}} \exp\left(-\frac{(Z^Q)^2}{2\sigma_{LN}^2}\right), -\infty \le A^Q < \infty \quad (34)$$

Where σ_{LN}^2 is the variance of the Lognormal fading channel as previously derived (19). Therefore, it can be seen that the amplitude of the channel's frequency response, denoted as |Z|, follows the Rayleigh distribution in the frequency response for previous channels. This may be mathematically represented as $|Z|=\sqrt{(Z^I)^2 + (Z^Q)^2}$.

In a 4-QAM scheme, the received signal that complex and noisy is represented as Y in the frequency domain, while the collection of all feasible modulated symbols X is indicated as C, where C = {C1, C2, C3, C4}. The bit error rate (BER) in the AWGN can be expressed as

$$P_b^{AWGN} = \frac{1}{2} erfc\left(\sqrt{\frac{E_b}{No}}\right) \quad (35)$$

And the BER over Rayleigh fading channel may be formulated as

$$P_b^{Rayleigh} = \frac{1}{2}\left[1 - \left(\frac{\sqrt{\frac{E_b}{2\sigma_U{}^2}}}{\sqrt{1+\frac{E_b}{2\sigma_u{}^2}}}\right)\right] \quad (36)$$

And the BER over Nakagami-m fading channel could be stated as [27]

$$P_b^{Nakagami-m} = \frac{1}{2}\left[1 - \left(\frac{\sqrt{\sigma_N^2\frac{E_b}{2\sigma_u{}^2}}}{\sqrt{1+\sigma_N^2\frac{E_b}{2\sigma_u{}^2}}}\right)\right] \quad (37)$$

5. BER computation over log-normal fading channel

In order to estimate the BER for QAM-OFDM over Log-normal fading channel in AWGN. The ratio of effective bit energy to noise is, $SNR = \gamma_b = \frac{|Z|^2 E_b}{N_0}$. Consequently, for a certain value of Z, the bit error conditional probability is

$$P_{b|Z} = \frac{1}{2} erfc\left(\sqrt{\gamma_b}\right) \quad (37)$$

Based on our analysis of the chi-square random variable, it can be inferred that a Rayleigh distributed random variable has two degrees of freedom, and can be expressed as,

$$p(\gamma_b) = \frac{1}{E_b/2\sigma_u{}^2} e^{\frac{\gamma_b}{E_b/2\sigma_u{}^2}}, \quad \gamma_b \ge 0 \quad (38)$$

Thus, the BER may be calculated as:

$$P_b^{\text{Log-normal}} = \int_0^\infty \frac{1}{2} erfc\sqrt{\gamma_b}\, p(\gamma_b) d\gamma_b$$
$$= \int_0^\infty \frac{1}{2} erfc\sqrt{\gamma_b}\, \frac{1}{E_b/2\sigma_u{}^2} e^{\frac{\gamma_b}{E_b/2\sigma_u{}^2}} d\gamma_b$$
$$= \frac{1}{2}\left[1 - \left(\frac{\sqrt{\sigma_{LN}^2\frac{E_b}{2\sigma_u{}^2}}}{\sqrt{1+\sigma_{LN}^2\frac{E_b}{2\sigma_u{}^2}}}\right)\right] \quad (39)$$

6. Numerical simulation and performance

The focus of this research is to evaluate the performance of a proposed NR-Polar-QAM-OFDM system in terms of bit error rate (BER) across various communication channels. Specifically, we investigate the Rayleigh channel, Nakagami-m channel, and Lognormal fading channel. The performance of the proposed system is compared against that of an uncoded QAM-OFDM system. The polar code and

Table 1. contains information of parameters

Modulation	**QAM**		
No. of sub-carriers	64		
No. of Block length	10000		
Channel model	Frequency selective Rayleigh fading channel Frequency selective Nakagami-m fading channel Frequency selective Lognormal fading channel		
Noise	AWGN		
Code rate	1/2 and 1/3		
n_{max} for PUCCH/PUSCH	10	n_{max} for PDCCH/PBCH	9
L for PUCCH/PUSCH	8,16	L for PDCCH/PBCH	8,16

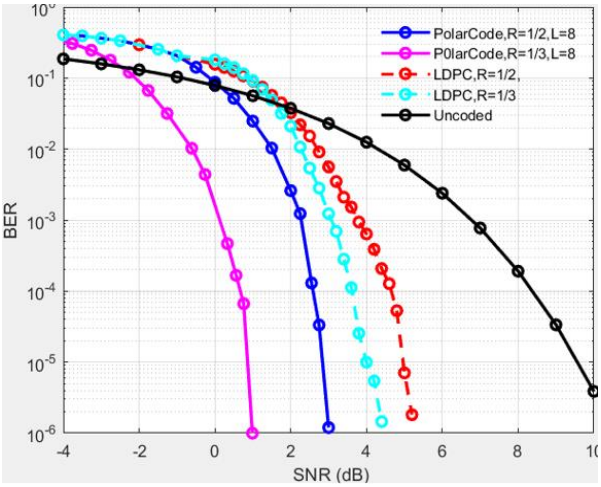

Figure. 5 BER of Polar- COFDM versus LDPC -COFDM systems with AWGN

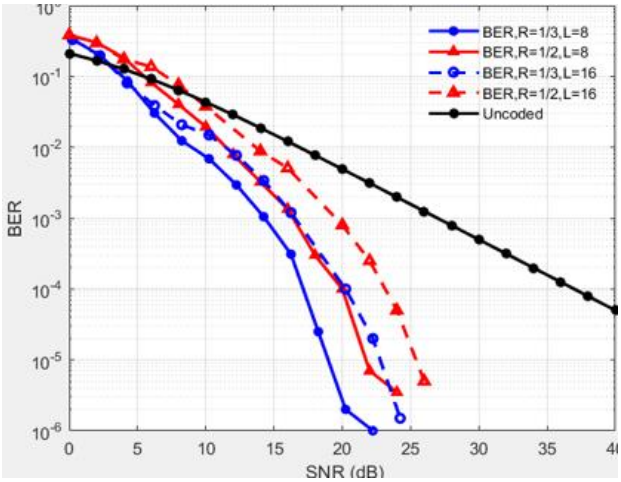

Figure. 6 BER of Polar- COFDM-QAM systems over Rayleigh fading channel.

channels stated above are utilized using the parameters listed in Table 1.

The mother polar code's code length, $N = 2^n$, must be determined as the first parameter. The formula used to determine

$n = max(\min(n_1, n_2, n_{max}), n_{min})$, where n_{max} The term "represent" serves as an upper limit on the mother code. While, $n_{min,}$ the term "represent" serves as a lower limit on the mother code. Performance of the new radio polar codes on the binary AWGN channel is shown in Fig. 5. Code lengths of 128/192 were simulated, and no rate matching was used, meaning that the transmitted length is the same as the code length. The amount of the simulated information ranged from 50 to 80, which is within the normal range of DCI size (with a 24-bit CRC) delivered through PDCCH in 5G specifications. The modulation order of the Physical Downlink Control Channel (PDCCH) employed for simulation was MQAM. The decoding method used is SCL decoding, with list sizes of 8 and 16. It is important to observe that, for any given code length, the necessary signal-to-noise ratio (SNR) consistently rises as the quantity of the information being sent grows. Specifically, In Fig. 5, we state a comparison between BER performance for both the Polar code and the LDPC code. The coding rates were first established at (1/2) for two different systems, and later they were fixed at (1/3) for the identical code lengths. Both systems' BER performance is compared to the results of an uncoded Monte Carlo simulation and a theoretically determined BER that was calculated using Eq. (34) It can be shown from the Fig. 5, that the proposed Nr-Polar COFDM outperforms the LDPC-COFDM by 3.25 dB at BER=10−5 and gives about 8.4 dB coding gain (CG) compared uncoded -OFDM scheme[27, 36].

The estimation of variances in the AWGN channel model is carried out by using Signal-to-Noise Ratio (SNR) measurements. In the scenario of fading presence, a fading channel block was accompanied by the AWGN channel block that had been used previously. Fig. 6 illustrate the performance analysis of the NR-Polar Code-QAM-OFDM system for two decoding list-bits (8 and 16), in comparison to the performance of the UOFDM system, under the influence of a Rayleigh fading channel.

The simulation outcomes demonstrate a close alignment between the theoretical bit error rate (BER) and the real BER for UOFDM over a Rayleigh channel with coding. In the end, it is found that channel coding has the ability to improve the system's BER performance. Therefore, in order to achieve a bit error rate of 10-6, it is necessary to have a coding gain for the OFDM system with PC

Table 2. Coded Gain

Rayleigh fading channel BER	E_b/N_0 dB				
	Uncoded OFDM system	Polar-COFDM	LDPC-COFDM	CGs Polar-COFDM	CGs LDPC-COFDM
10^{-3}	26.5 dB	14dB	8.8 dB	12.5 dB	17.7 dB
10^{-4}	38.5 dB	17.5dB	9.25 dB	21 dB	29.15dB
10^{-5}	48.5dB	19dB	0.5 dB	29.5 dB	38.dB
10^{-6}	58.5 dB	22.5dB	1.5 dB	36 dB	47dB

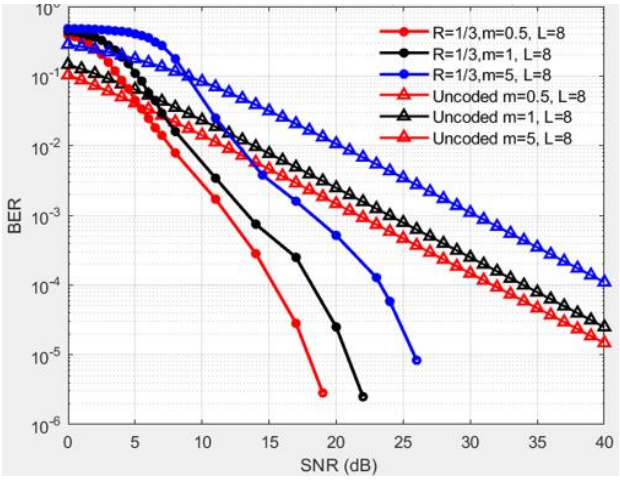

Figure. 7 BER performance of Polar Code / QAM-OFDM over Nakagami-m fading channel(R=1/3)

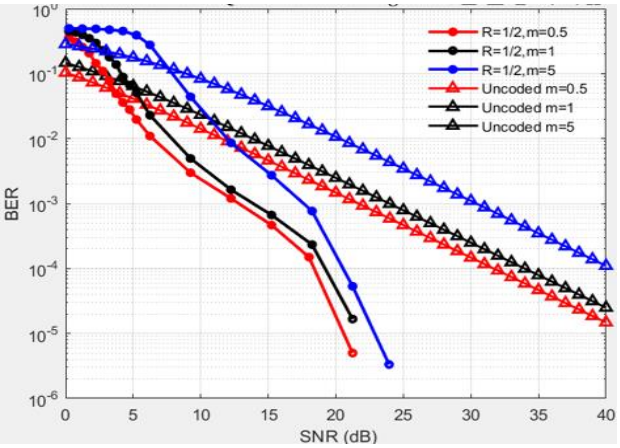

Figure. 8 BER performance of Polar Code / QAM-OFDM over Nakagami-m fading channel(R=1/2)

decoding. It is evident that the performance of polar coding with CRC assisted SCL decoding, with a list size (L) of 8, does not exceed performance of a system using LDPC coding [27, 36]. Examples of numerical comparisons between two codes in terms of coded gains are provided in Table 2.

The references [36, 37, and 38] have been used for the purpose of comparison. By comparing the performance of the proposed NR-Polar Code-QAM-OFDM system against the results obtained from the PCOFDM system described in reference [36], both codes utilize a rate of R = 0.5 and a block length N of 10000. When operating over an AWGN channel with a BER ≈ 10-5, the proposed system can achieve a 1.5 dB/bit reduction in SNR with BPSK mapping and a 4.2 dB/bit decrease in SNR with 4-QAM mapping [37]. Similarly, the simulation results displayed in Fig. 6 unambiguously demonstrate the superiority of the proposed NR-Polar Code-QAM-OFDM system over a frequency selective Rayleigh fading channel at an SNR of 23 dB in comparison to the results for the PCOFDM system given in [37] by gain of 10 dB at BER ≈ 10-5 with the BPSK modulation scheme and by gain of 12 dB with 4-QAM modulation at BER ≈ 5×10-5[37]. Additionally, similar results are obtained when comparing with reference [38,39] approximately.

The performance analysis of the NR-Polar Code-QAM-OFDM system, including both rates, is shown in Figures 7 and 8. These Figures illustrate the system's performance in the presence of a Nakagami-m fading channel. The results of this analysis is evaluated in relation to the UOFDM system's BER performance.

The usage of Polar Code-OFDM over UOFDM, with the latter producing better coding enhancements, resulted in a substantial boost in system performance. Based on the analysis of Fig. 7 and 8, it is evident that the design system scheme, exhibits a much high- er coding gain of about 14 dB, compared to the UOF-DM system. This observation holds true for a shaping factor (m) of 0.5 and a BER of 10-4, under the influence of a Nakagami-m fading channel.

The usage of Polar Code-OFDM over UOFDM, with the latter producing better coding enhancements, resulted in a substantial boost in system performance. Based on the analysis of Figures 7 and 8, it is evident that the design system scheme, exhibits a much higher coding gain of about 14 dB, compared to the UOFDM system. This observation holds true for a shaping factor (m) of 0.5 and a BER of 10-4, under the influence of a Nakagami-m fading channel. The Fig. 8 demonstrate that the suggested system performs better when m falls in every situation. For instance, for BER=10-5, the system achieves approximately, CGs of 28.25, 25.4 and 40.15 dB for m = 0.5, 1 and 10, respectively. Moreover, the results obtained by using Monte Carlo simulation methods demonstrate a strong resemblance to the theoretical performance of the UOFDM system under identical conditions. Fig. 9 and 10 demonstrate the performance of the NR-Polar Code-QAM-OFDM system at different coding rates in the presence BAWGN. In this Figures, perform simulations to evaluate the performance of a design system under different conditions. Specific- ally, we examine the

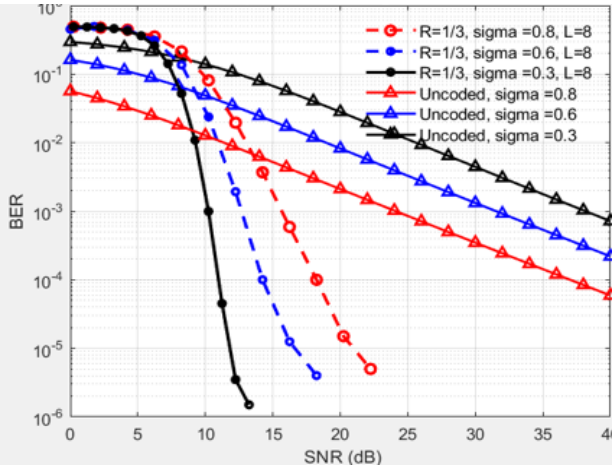

Figure. 9 BER performance of Polar Code / QAM-OFDM over Lognormal fading channel(R=1/3)

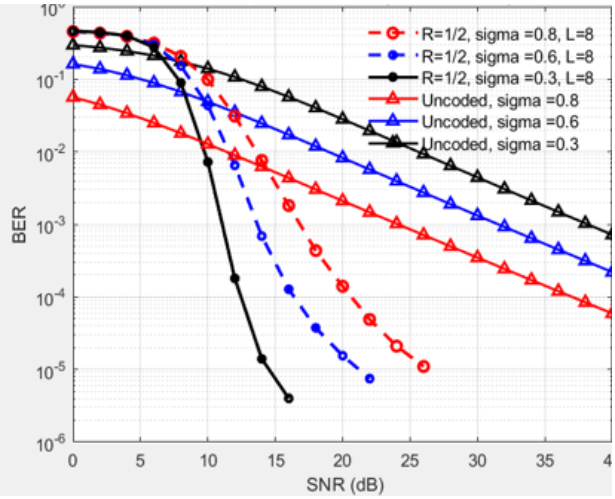

Figure. 10 BER performance of Polar Code / QAM-OFDM over Lognormal fading channel (1/2)

system's performance for both with and without channel coding over a Lognormal fading channel with varying levels of standard deviation (sigma = 0.3, 0.6, and 0.8) at both scenarios of coding rates. It is evident that within the lower SNR range of 0 to 10.5 dB, the systems using NR-Polar codes exhibit worse performance compared to those without any coding scheme. The rationale for this is because the SNR is sufficiently low, resulting in a rather high error rate for the channel coding. Consequently, attempting error correction would be counterproductive. However, the performance of average BER in QAM -OFDM systems has been significantly enhanced in the higher SNR area by the utilizing of polar codes. As an instance, it can be seen that the use of proposed Polar-COFDM when combined with SCL decoding (with a list size of 8) results in a coding gain of about 48.3 dB and 43, 37 at rate (1/3) and rate (1/2) respectively, higher than that of UOFDM, considering BER of around 10-5 in the case of (sigma= 0.3). In addition, the use of CRC in the SCL decoding algorithm has been shown to significantly decrease the BER of the system.

7. Conclusion

The multipath fading channel is taken into account in this research while evaluating how well the NR- Polar- COFDM system performs. The Rayleigh channel model, the Nakagami-m model and Lognormal fading channel are used in order to include the many parameters that lead to signal distortion inside the channel. Using Monte Carlo simulations, we discover that under Rayleigh, Nakagami-m, and Lognormal fading channel conditions, the QAM constellation NR-Polar-COFDM has been enhanced in term of coding gain in comparison to the uncoded OFDM system by using the LLRs calculated from generated noise PDFs at the ZF equalizer output via the different scenario channels. Moreover, it has been shown that the polar -COFDM system, when combined with CRC assisted SCL decoding, is not superior performance compared to the LDPC coded OFDM system in practice.

In the context of the Nakagami-m channel model, a reduction in the shaping factor m leads to improved system performance. However, it is important to note that this improvement is accompanied with a fall in coding gain. This decrease may be attributed to the fact that the signal intensity experiences reduced fluctuations compared to the scenario of Rayleigh fading, specifically when m is equal to 1. In simulations of the NR-Polar Code-QAM-OFDM system operating in AWGN under the Lognormal fading channel, a range of standard deviations (sigma = 0.3, 0.6, and 0.8) have been evaluated. The findings demonstrate that for higher values of SNR, the Lognormal fading channel has better coding gain than the other fading channels as sigma falls.

Conflicts of Interest

The authors declare that there is no conflict of interests regarding the publication of this paper.

Author Contributions

The First author’s contributions include many key aspects, including the development of the technique, creation of the software, drafting the first manuscript, overseeing project management, and doing formal analysis. The second author's participation encompasses the validation and the investigation, as well as providing supervision.

Acknowledgments

This work is supported by the college of Engineering/ Mustansiriyah University Iraq, Baghdad. (https://webmail.uomustansiriyah.edu.iq).

References

[1] E. Arikan, "Channel polarization: A method for constructing capacity achieving codes for symmetric binary-input memoryless channels", *IEEE Transactions on Information Theory*, Vol. 55, No. 7, pp. 3051-3073, 2009.

[2] 3rd Generation Partnership Project (3GPP), *Multiplexing and channel coding*, 3GPP 38.212 V.15.3.0, 2018.

[3] N. Hou, K. Niu, Z. He and S. Sun, "Test and performance analysis of PUSCH channel of LTE system", In: *Proc. of 2013 5th IEEE International Symposium on Microwave*, Antenna, Propagation and EMC Technologies for Wireless Communications, Chengdu, China, pp. 110-114, 2013, doi: 10.1109/MAPE.2013.6689964.

[4] T. Levanen, K. Ranta-Aho, K. Pajukoski, M. Renfors, and M. Valkama, "5G new radio uplink performance: Noise, interference and emission constraints", In: *Proc. of 2018 IEEE Wireless Communications and Networking Conference (WCNC)*, Barcelona, Spain, pp. 1-6, 2018, doi: 10.1109/ WCNC.2018.8377161.

[5] F. Di Stasio, M. Mondin, and F. Daneshgaran, "Multirate 5G Downlink Performance Comparison for f-OFDM and w-OFDM Schemes with Different Numerologies", In: *Proc. of 2018 International Symposium on Networks*, Computers and Communications (ISNCC), Rome, Italy, pp. 1-6, 2018, doi: 10.1109/ISNCC.2018.8530905.

[6] 3GPP TS 38.211, *NR; Physical Channels and Modulation*, version 15.0.0, 2017.

[7] 3GPP TS 38.212, *NR; Multiplexing and Channel Coding*, version 15.0.0, 2017.

[8] E. Arikan, "A performance comparison of polar codes and Reed-Muller codes", *IEEE Communications Letters*, Vol. 12, No. 6, pp. 447-449, 2008, doi: 10.1109 /LCOMM. 2008. 0800- 17.

[9] Y. Zhang, A. Liu, K. Pan, C. Gong, and S. Yang, "A practical construction method for polar codes", In: *Proc. of IEEE Communication Letters*, Vol. 18, No. 11, pp. 1871-1874, 2014.

[10] I. Tal and A. Vardy, "How to Construct Polar Codes", *IEEE Transactions on Information Theory*, Vol. 59, No. 10, pp. 6562-6582, 2013, doi: 10.1109/TIT.2013.2272694.

[11] R. Mori and T. Tanaka, "Performance of Polar Codes with the Construction using Density Evolution", In: *Proc. of IEEE Communications Letters*, Vol. 13, No. 7, pp. 519-521, 2009, doi: 10.1109/LCOMM.2009.090428.

[12] R. Mori and T. Tanaka, "Performance and construction of polar codes on symmetric binary-input memoryless channels", In: *Proc. of 2009 IEEE International Symposium on Information Theory*, Seoul, Korea (South), pp. 1496-1500, 2009, doi: 10.1109/ISIT.2009.5205857.

[13] E. Arikan, "Systematic Polar Coding", In: *Proc. of IEEE Communications Letters*, Vol. 15, No. 8, pp. 860-862, 2011, doi: 10.1109/LCO MM. 2011.061611.110862.

[14] G. Sarkis, P. Giard, A. Vardy, C. Thibeault and W. J. Gross, "Fast Polar Decoders: Algorithm and Implementation", In: *Proc. of IEEE Journal on Selected Areas in Communications*, Vol. 32, No. 5, pp. 946-957, 2014, doi: 10.1109/JSAC.2014.140514.

[15] V. G. Tikka and R. Sivashanmugam, "Error Correction Using Hybrid Coding Algorithm for BER Reduction in MIMO-OFDM", *International Journal of Intelligent Engineering and Systems*, Vol. 15, No. 6, pp. 618-626, 2022, doi: 10.22266/ijies2022.1231.55.

[16] G.A. Al-Rubaye, C. C. Tsimenidis, and M. Johnston, "Low-density parity check coded orthogonal frequency division multiplexing for PLC in non-Gaussian noise using LLRs derived from effective noise probability density functions", *IET Communications*, pp. 2425-2432, 2017, doi: 10.1049/iet-com.2017. 0265.

[17] A. A. Andi and O. Gazi, "Fast decoding of polar codes using tree structure", *IET Communications*, 2019, doi: 10.1049/iet-com.201 8. 5019.

[18] I. Tal and A. Vardy, "List Decoding of Polar Codes", In: *Proc. of IEEE Transactions on Information Theory*, Vol. 61, No. 5, pp. 2213-2226, 2015, doi: 10.1109/TIT.2015.2410251.

[19] R. Bose, *Information Theory, Coding and Cryptography*, 2nd Edition, Tata McGraw Hill, 2008.

[20] 3GPP, TS 138 212, *5G; NR; Multiplexing and channel coding*, Version 16.2.0, Release 16, 2020.

[21] S. Tanangsanakool, P. Reangsuntea, K. Mori, and P. Boonsrimuang, "Low-Complexity based TDE Method for OFDM Signal in Higher Time-Varying Fading Channel", *International Journal of Intelligent Engineering and Systems*, Vol.13, No. 6, pp. 21-32, 2020, doi: 10.22266/ijies2020.0831.03.

[22] G.A. Al-Rubaye, Charalampos C. Tsimenidis, and Martin Johnston, "Improved performance of TC-OFDM-PLNC for PLCs using exact derived impulsive noise pdfs", In: *Proc. of 2017 IEEE International Conference on Communications Workshops (ICC Workshops)*, 2017.

[23] M. Nakagami, "The m-distribution - A General Formula of Intensity Distribution of Rapid Fading", In: *Proc. of Statistical Methods in Radio Wave Propagation*, No. 2. Pergamon Press INC., pp.3-36, 1958, doi: 10.1016/B978-0-08-009306-2.50005-4.

[24] G. A. Al-Rubaye, C. C. Tsimenidis, and M. Johnston, "Performance evaluation of T-COFDM under combined noise in PLC with log-normal channel gain using exact derived noise distributions", *IET Commun.*, Vol. 13, No. 6, pp. 766–775, 2019, doi: 10.1049/iet-com.2018.6185.

[25] V. M. Artyushenko and V. I. Volovach, "Nakagami Distribution Parameters Comparatively Estimated by the Moment and Max imum Likelihood Methods", *Optoelectron. Instrument and data Proc*, Vol. 55, No. 3, pp. 237-242, 2019. doi.org/10.3103/ S8756699 01903004 X.

[26] U. Charash, "Reception through Nakagami fading multipath channels with random delays", *IEEE Trans. Commun.*, Vol. COM-27, pp. 657470, Apr. 1979.

[27] M. H. Ali, and G. A. Al-Rubaye, "Performance Analysis of 5G New Radio LDPC over Different Multipath Fading Channel Models", *International Journal of Computer Network and Information Security (IJCNIS)*, Vol. 15, No.4, pp.1-12, 2023, doi:10.5815/ijcnis. 20 23. 04.01.

[28] S. Kumar, P.K. Gupta, G. Singh, and D. S. Chauhan, "Performance Analysis of Rayleigh and Rician Fading Channel Models using Matlab Simulation", *International Journal of Intelligent Systems and Applications (IJISA)*, Vol.5, No.9, pp.94-102, 2013, doi: 10.5815/ ijisa.2013.09.11.

[29] Z. K. Adeyemo, S. I. Ojo, S. B. Ebinaiye, and O. F. Oseni, "Development of a Hybridized Diversity Combiner over Nakagami Fading Channel", *International Journal of Information Engineering and Electronic Business (IJIEEB)*, Vol.11, No.3, pp. 45-53, 2019, doi: 10.5815/ ijieeb.2019.03.06.

[30] Q. Tuan, N., Nguyen, DT. & Cong, L.S. "A 10-state model for an AMC scheme with repetition coding in mobile wireless networks", *J Wireless Com Network 2013*, doi: 10.1186/1687-1499-2013-219.

[31] H. Suzuki, "A statistical model for urban radio propagation", *IEEE Trans. on Commun.*, Vol. COM-25, pp. 673-680,1977.

[32] M. K. Simon, *Digital Communication over Fading Channel*, Second Edition. John Wiley & Sons, INC., Publication, 2005.

[33] K. R. Gajulapalli and M.S. Gnanadhas, "Analysis of PAPR and BER Reduction in MIMO- OFDM using Hybrid Moth Flame-Improved Firefly Algorithm", *International Journal of Intelligent Engineering and Systems*, Vol. 15, No. 4, pp. 97-105, 2022, doi: 10.22266/ijies2022.0831.10.

[34] K. Sun and M. Jiang, "A hybrid decoding algorithm for low-rate LDPC codes in 5G", In: *Proc. of 10th Int. Conf. Wireless Commun. Signal Process. (WCSP)*, Hangzhou, China, pp. 1-5. 2018.

[35] B. Tahir, S. Schwarz, and M. Rupp, "BER comparison between Convolutional, Turbo, LDPC, and Polar codes", In: *Proc. of 2017 24th International Conference on Telecommunications (ICT)*, pp. 1-7, 2017, doi: 10.1109/ ICT.2017. 7998249.

[36] R. Benkhouya, I. Chana and Y. Hadi, "Evaluation of the polar coded OFDM system", In: *Proc. of 2017 International Conference on Wireless Networks and Mobile Communications (WINCOM)*, Rabat, Morocco, pp. 1-5, 2017, doi: 10.1109/WINCOM.2017.8238148.

[37] R. Umar, F. Yang and S. Mughal, "BER performance of a polar coded OFDM over different channel models", In: *Proc. of 2018 15th Inter- national Bhurban Conference on Applied Sciences and Technology (IBCAST), Islamabad*, Pakistan, pp. 764-769, 2018, doi: 10.1109/IBCAST.2018.8312308.

[38] M. Meenalakshmi, S. Chaturvedi and V. K. Dwivedi, "Performance Analysis of Polar Codes in 5G New Radio", In: *Proc. of 2021 7th International Conference on Signal Processing and Communication (ICSC), Noida*, India, 2021, pp. 96-99, 2021, doi: 10.1109/ ICSC53193. 2021.9673290.

[39] I. El Kaime, A. A. Madi and H. Erguig, "Systematic Polar Codes in 5G NR", In: *Proc. of 2022 2nd International Conference on Innovative Research in Applied Science*, Engineering and Technology (IRASET), Meknes, Morocco, pp. 1-5, 2022, doi: 10.1109/IRASET52964 .2022. 9738221.